Πρακτικά	3ου Συνέδριου	Μάϊος 1986	
Δελτ. Ελλ. Γεωλ. Εταιρ.	Τομ. XX/3	σελ. 255-269	Αθήνα 1988
Bull. Geol. Soc. Greece	Vol.	pag.	Athens

RUTPURE COMPLEXITY AND FAULT ASPERITIES: THE KORINTH, CENTRAL GREECE, EARTHQUAKE SEQUENCE OF 1981

G. STAVRAKAKIS*, J. DRAKOPOULOS**, K. MAKROPOULOS**

ABSTRACT

Teleseismic long period P-waves recorded by WWSSN stations from the 24 February 1981 Gulf of Corinth earthquake (Ms=6.7) and its principal aftershocks of 25 February (Ms=6.4) and 4 March (Ms=6.4) are iteratively deconvolved in order to investigate the degree of complexity of the rupture and to extract information about asperities or barriers on the fault plane.

A far-field displacement source time function with the rise time τ=3sec and process time tc=6sec for the main shock, τ=1.5sec and tc=3sec for the 25 February shock, and τ=3sec and tc=7sec for the 4 March shock is obtained.

INTRODUCTION

The purpose of this study is to give a better understanding of the detailed sequence of the individual subevents during fault rupture associated with strong earthquakes. The 24 February 1981, Corinth, central Greece, earthquake (Ms=6.7) and its principal aftershocks of magnitude Ms-6.4 on 25 February and 4 March have been chosen because this earthquake sequence was accompanied by surface faulting and each event gave rise to complex body waves which were well recorded at WWSSN stations.

Several recent observations indicate, that many earthquakes are in fact complex or multiple events (WYSS and BRUNE, 1967; WU and KANAMORI, 1975; FUKAO and FURUMOTO, 1975). Complex events have also been proposed in the numerical modeling of faulting with variable strength by DAS and AKI, 1977; MIKUMO and MIYATAKE, 1978. From the study of rupture propagation using strong motion data (MORI and SHIMAZAKI, 1984) as well as far-field seismograms (LANGSTON and HELMBERGER, 1975; CIPAR, 1979; LAY and KANAMORI, 1980; CHUNG and CIPAR, 1983) it is widely accepted that strong earthquakes consist of a sequence of small individual subevents.

In order to extract information about asperities or barriers on the

* Earthquake Planning and Protection Organization, Athens.
** Seismological Laboratory, University of Athens, Athens.

fault plane and the details of rupture propagation of the Corinth earthquake sequence, the inversion method of complex P-waves developed by KIKUCHI and KANAMORI (1982) and recently reaffirmed by KIKUCHI and SUDO (1984) is applied.

DATA ANALYSIS AND RESULTS

Teleseismic P-waves recorded at WWSSN stations are used in this study. Only stations in the epicentral distance range 45° to 90° are used in order to minimize complications due to upper mantle structure and core effects. The effect of anelastic attenuation is taken into account using Futterman's Q-operator, parameterized by the quantity T/Q (travel time divided by the average Q along the path). The geometrical spreading factor and the emergent angle are also computed for each station. The instrumental responses of WWSSN seismographs are obtained by using Hagiwara's method.

Following KIKUCHI and KANAMORI (1982) the data is inverted from all stations used (multi-station analysis) to obtain the far-field source time function as well as the seismic moment, onset time, and location of the individual subevents which occured during the rupture. A linear ramp function with rise time τ and process time tc is used. The fault plane is divided into N points in the strike direction and into M points in the dip direction in order to compute synthetic wavelets generated from unit douple-couple point sources at all possible locations.

For given source mechanism, the point sources at a hypocenter are placed in a homogeneous half-space and the wavelets following the method by KANAMORI and STEWART (1978) are calculated with Vp=6.0km/sec for the P-wave velocity, 2.7gr/cm^3 for the density and T/Q=1.0. The inversion is performed with 25 iterations until no more significant decrease in the residual error occurs and while varing the rise time and process time in the least square sense. Further details for each event are described separately in the sections that follow.

Analysis of the main shock. Figure 1 shows the relocated epicenters (JACKSON et al., 1982; PAPAZACHOS et al., 1984) of the main shock and its principal aftershocks in addition to the focal mechanism obtained by DZIEWONSKI and WOODHOUSE (1983) from centroid-moment tensor solution. The northwest-striking nodal plane with strike, φ=283°, dip angle, δ=44°, and rake angle, λ=-72° is considered to be the fault plane because the surface expression of this plane is the western part of the southern fracture (PAPAZACHOS et al., 1984). KIM et al.,(1984)(suggest a slightly different solution for the fault plane with strike 285°, dip 40°N and rake angle-70°) based on the first P-wave motion and the best fit of SH synthetics.

The fault plane is divided into 10x5 grid points with an equal spacing of 5 km and the wavelets are calculated by taking the time shifts into account. A subevent sequence with different onset time, location on the fault plane, and seismic moment is then obtained by an iterative deconvolution of the observed P-wave seismograms. P-wave sunthetics for a trapezoidal source time function with (τ, tc) = (3,6) sec provides the best solution. The douple-couple point source is placed at the depth of 8km. For these values an approximation error Δ_{25}=29% is obtained. The inferred source time function, the moment rate function and the normalized approximation error are shown in Figure 2. Subevents 1,2,3, and 4 are identified as marked in Figure 2a. The revealed parameters of all subevents are listed in Table 1.

The spatial distribution of the significant subevents on the fault plane is shown in Figure 3. The height of the squares correspond to the seismic moment.

In Figure 4, the resulting synthetic wave forms are compared with the observed ones. The matching is satisfactory at all stations.

In summarizing the obtained results, one concludes that the rupture sequence of the main shock can be represented by the sequential occurrence of approximately 4 significant subevents with time separations varying from 3 to 8 sec. If an average rupture velocity of about 2.5km/sec is assumed this temporal separation corresponds roughly to a spatial separation of 7.5 to 20 km which represents the size of asperities or barriers on the fault plane.

Analysis of the shock of 25 February.

Figure 1 shows the location and the focal mechanism of the first large aftershock (Ms=6.4) of February 25. The fault plane solution is also obtained by DZIEWONSKI and WOODHOUSE (1983). The dipping NW plane with strike φ=261°, dip=40°. and rake angle λ=-74°is taken as the fault plane because it is consistent with the strike and slip direction of the eastern part of the southern lines (PAPAZACHOS et al., 1984).

The iterative deconvolution procedure is repeated in the same manner as for the main shock. The best solution, with an approximation error Δ_{25}= 25%, is obtained by a source time function with rise time τ=1.5sec and process time tc=3sec at a depth of 6km.

The inferred source time function and moment rate function are shown in Fig.5. Their shape is much more complex than that of the main shock which implies that the rupture mechanism of this shock is quite different

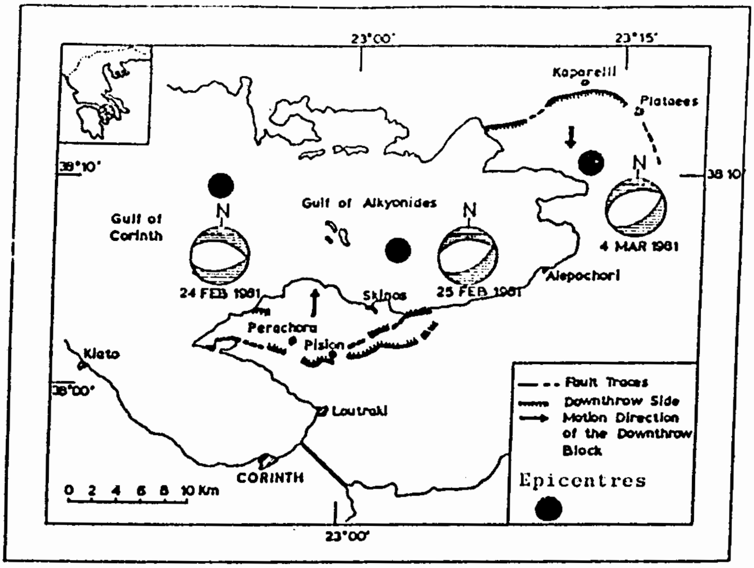

FIGURE 1: Map of epicentral area showing surface ruptures (modified from Papazachos et al., 1984).

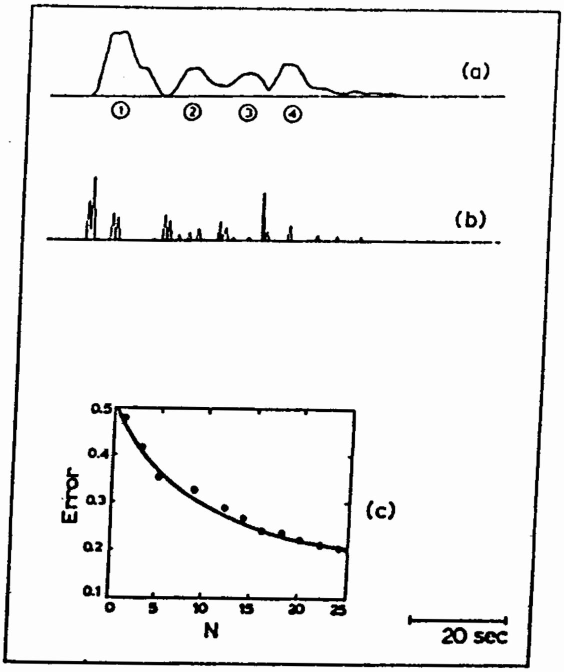

FIGURE 2: Main shock of the 24 February, 1981: (a) source time function, (b) moment rate function, and (c) normalized approximation error versus number of iterations (for multi-station data).

TABLE 1 : Main shock of the 24 February, 1981. Subevent sequence on the fault plane.

No	Onset time(S)	Location X(km)	Location Y(Km)	Seismic Moment rate ($x10^{25}$dyne cm)	Seismic Moment ($x10^{25}$dyne.cm)
1	3.5	-12.0	-18.0	0.259E-01	0.1298E+00
2	3.5	18.0	-12.0	0.189E+00	0.9464E+00
3	3.5	-6.0	6.0	0.134E+00	0.6711E+00
4	4.0	12.0	-12.0	0.527E-01	0.2636E+00
5	7.5	6.0	-6.0	0.631E-01	0.3156E+00
6	8,5	-24.0	-12.0	0.606E-01	0.3033E+00
7	8.5	-18.0	-12.0	0.476E-01	0.2380E+00
8	12.0	6.0	6.0	0.268E-01	0.1342E+00
9	12.0	-6.0	-18.0	0.106E+00	0.5303E+00
10	19.0	30.0	-18.0	0.298E-01	0.1482E+00
11	20.0	-18.0	0.0	0.436E-01	0.2181E+00
12	21.0	30.0	-12.0	0.620E-01	0.3104E+00
13	21.5	30.0	-12.0	0.504E-01	0.2521E+00
14	22.5	12.0	6.0	0.205E-01	0.1029E+00
15	22.5	-12.0	0.0	0.169E-01	0.8478E-01
16	27.0	-24.0	-12.0	0.434E-01	0.2175E+00
17	32.5	30.0	-12.0	0.731E-01	0.3659E+00
18	34.5	30.0	6.0	0.156E-01	0.7833E-01
19	34.5	30.0	-12.0	0.421E-01	0.2108E+00
20	35.5	6.0	-6.0	0.423E-01	0.2116E+00
21	39.5	12.0	0.0	0.161E-01	0.8073E-01
22	42.0	12.0	-12.0	0.134E+00	0.6699E+00
23	47.5	30.0	-18.0	0.501E-01	0.2506E+00
24	55.0	6.0	6.0	0.945E-02	0.4727E-01
25	62.5	-24.0	-12.0	0.474E-01	0.2371E+00

TOTAL SEISMIC MOMENT=$7.02x10^{25}$

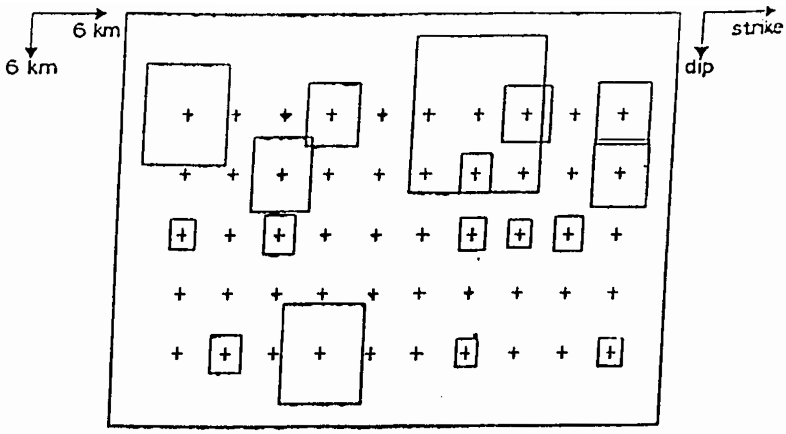

FIGURE 3: Main shock of the February 24, 1981. Spatial distribution of the individual subevents on the fault plane as obtained by the inversion method.

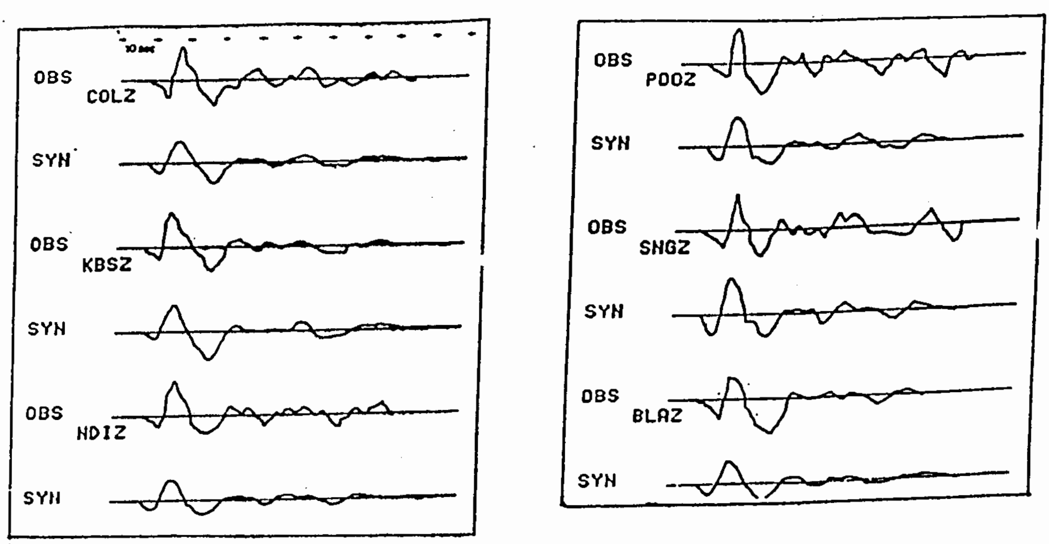

FIGURE 4 : The 1981 Corinth earthquake sequence (aftershock of the 24 February): Comparison between observed and synthetic seismograms.

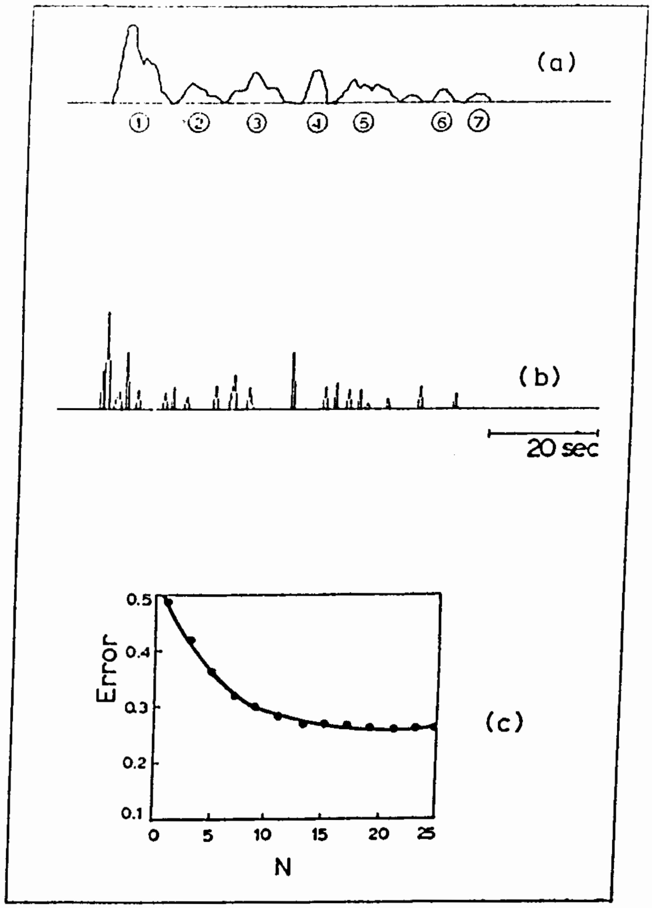

FIGURE 5: Aftershock of the 25 February, 1981: (a) Source time function, (b) moment rate function, and (c) normalized approximation error versus number of iterations (for multi-station data).

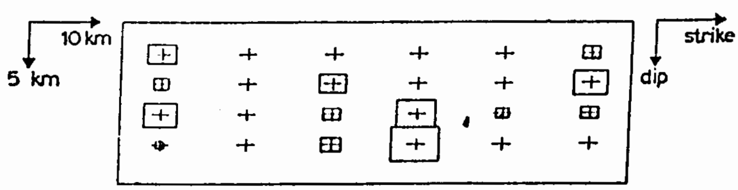

FIGURE 6: Aftershock of the 25 February, 1981. Spatial distribution of the individual subevents on the fault plane as obtained by the inversion method.

the main shock. Seven significant individual shocks are identified as marked in Figure 5a. The spatial distribution of all subevents is shown in Figure 6. Their parameters are listed in Table 2. As it can be shown, the first stage of the rupture includes 3 relatively large subevents with seismic moments $1.1x10^{24}$, $2.9x10^{24}$, and $1.6x10^{24}$ dyne.cm, respectively. The total seismic moment of the multiple sequence ammounts to $1.78x10^{25}$ dyne.cm. After a quiescence of about 10 sec the last large subevent occured with a seismic moment of $1.4x10^{24}$ dyne.cm. It should be noted that at the final stage only minor subevents occured which may be regarded as a sort of aftershocks. In Fig.7 the synthetic seismograms are compared with the observed ones.

Analysis of the shock of 4 March.

The location and the focal mechanism of this shock is shown again in Figure 1. The nodal plane with strike φ=246°, dip=41°, and rake λ=-84° (DZIEWONSKI and WOODHOUSE, 1983) is considered to be the fault plane because this is in agreement with the slip direction of the northern fracture line (PAPAZACHOS et al., 1984). A trapezoidal far-field source time function with rise time τ=3sec and process time tc=7sec is used to compute the synthetic P-wave seismograms. The douple-couple point sources are placed at a depth of 6 km. With these values an approximation error Δ_{25}=16% is obtained.

Following the same procedure the source time function and the moment rate function are obtained as shown in Figure 8. Their shape is also complex and six individual subevents are shown in Fig. 8a. The rupture process of this shock seems to be different from that of the main event and the first large aftershock as well.

The spatial distribution of all subevents is shown in Figure 9. At the first stage of the rupture occured only one significant subevent followed by numerous smaller ones without directivity nor clustering in space. It should also be noted, that four subevents took place on the upper part of the fault plane and they may be responsible for the observed breaks in the northern fracture line (Fig. 1). In the Fig. 10, the resultant synthetic seismograms are compared with the observed ones.

DISCUSSION

In this paper, the investigation of the source process of the main shock of the February 24, 1981, Corinth, central Greece earthquake and its two principal aftershocks was conducted by applying Kikuchi and Kanamori's (1982) method.

TABLE 2: Aftershock of the 25 February, 1981. Subevent sequence on the fault plane.

No	Onset time(S)	Location X(km)	Y(km)	Seismic Moment rate ($x10^{25}$dyne cm)	Seismic Moment ($x10^{25}$dyne.cm)
1	1.5	10.0	0.0	0.3885E-01	0.1166E+00
2	2.4	10.0	5.0	0.9758E-01	0.2927E+00
3	3.9	20.0	0.0	0.1162E-01	0.3485E-01
4	4.4	-20.0	0.0	0.1858E-01	0.5573E-01
5	5.9	10.0	0.0	0.5652E-01	0.1696E+00
6	7.8	-20.0	0.0	0.1944E-01	0.5831E-01
7	12.7	-20.0	-5.0	0.1650E-01	0.4949E-01
8	14.2	30.0	-10.0	0.2176E-01	0.6528E-01
9	16.7	-20.0	-10.0	0.1248E-01	0.3743E-01
10	21.6	10.0	5.0	0.2316E-01	0.6947E-01
11	24.5	30.0	0.0	0.1833E-01	0.5498E-01
12	25.0	-20.0	0.0	0.1367E-01	0.4101E-01
13	25.0	30.0	-5.0	0.2167E-01	0.6500E-01
14	27.9	-20.0	0.0	0.2169E-01	0.6507E-01
15	28.4	-20.0	5.0	0.5368E-02	0.1611E-01
16	35.8	30.0	-5.0	0.4793E-01	0.1438E+00
17	35.8	-20.0	-10.0	0.9803E-02	0.2941E-01
18	41.6	0.0	-5.0	0.2264E-01	0.6792E-01
19	43.6	-20.0	-10.0	0.2601E-01	0.7803E-01
20	46.1	0.0	-5.0	0.1914E-01	0.5741E-01
21	48.0	0.0	0.0	0.1906E-01	0.5717E-01
22	49.5	-20.0	-10.0	0.4853E-02	0.1456E-01
23	52.9	0.0	5.0	0.1171E-02	0.3513E-01
24	58.8	10.0	5.0	0.2248E-01	0.6743E-01
25	65.2	0.0	5.0	0.1568E-01	0.4703E-01

TOTAL SEISMIC MOMENT=$1.7x10^{25}$

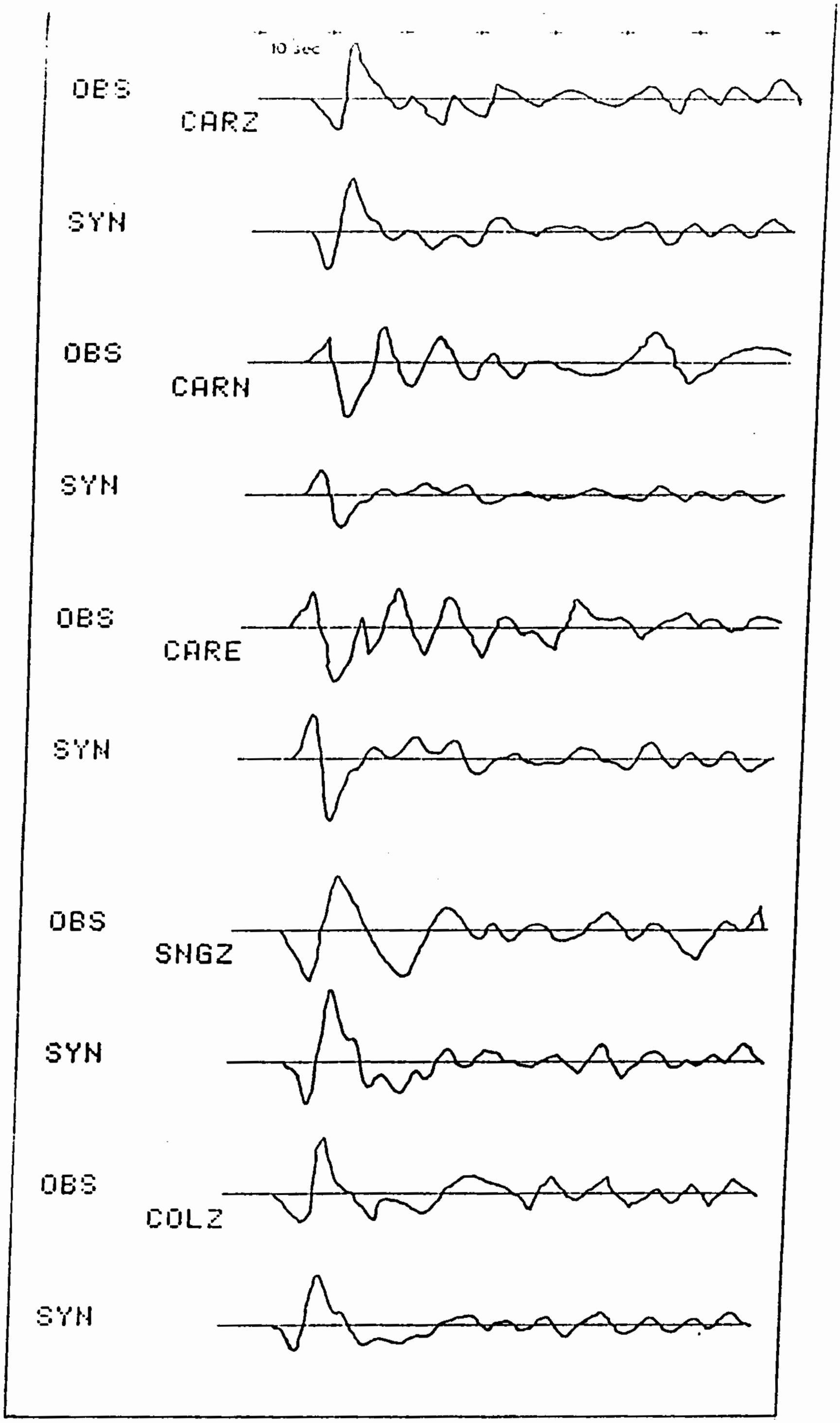

FIGURE 7 : The 1981 Corinth earthquake sequence (aftershock of the 25 February). Comparison between observed and synthetic seismograms.

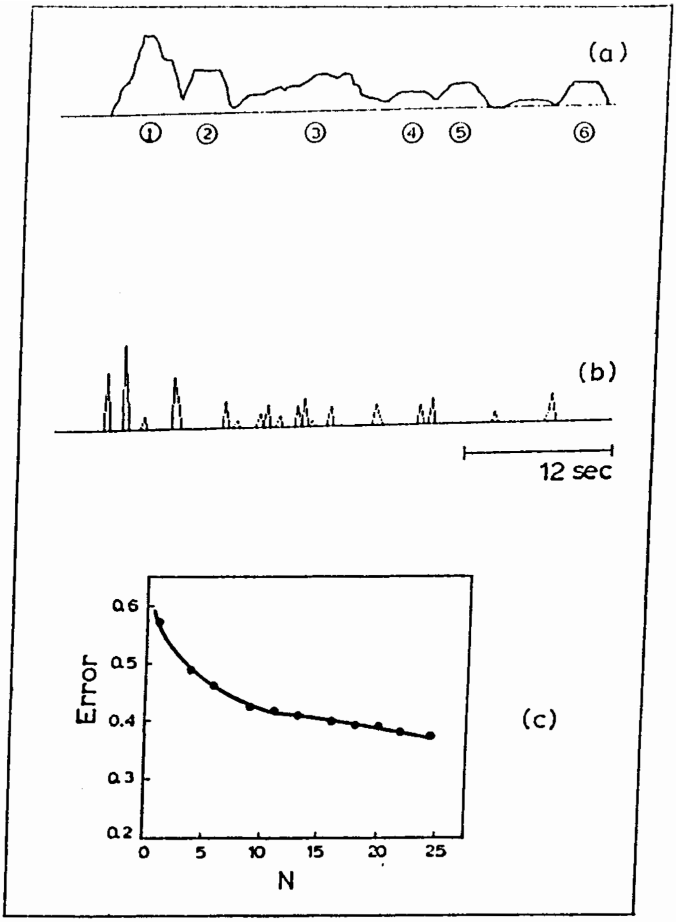

FIGURE 8 : The Corinth earthquake sequence (aftershock of the 4 March): (a) source time function, (b) moment rate function, and (c) normalized approximation error (for multi-station data).

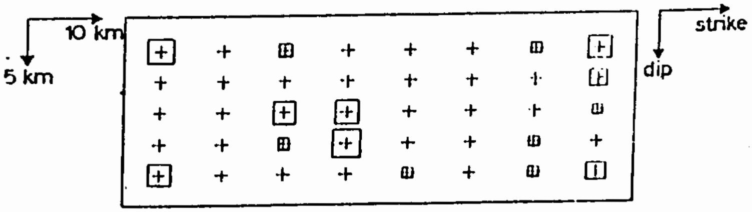

FIGURE 9 : The 1981 Corinth earthquake sequence (aftershock of the 4 March). Spatial distribution of the individual subevents on the fault plane as obtained by the inversion method.

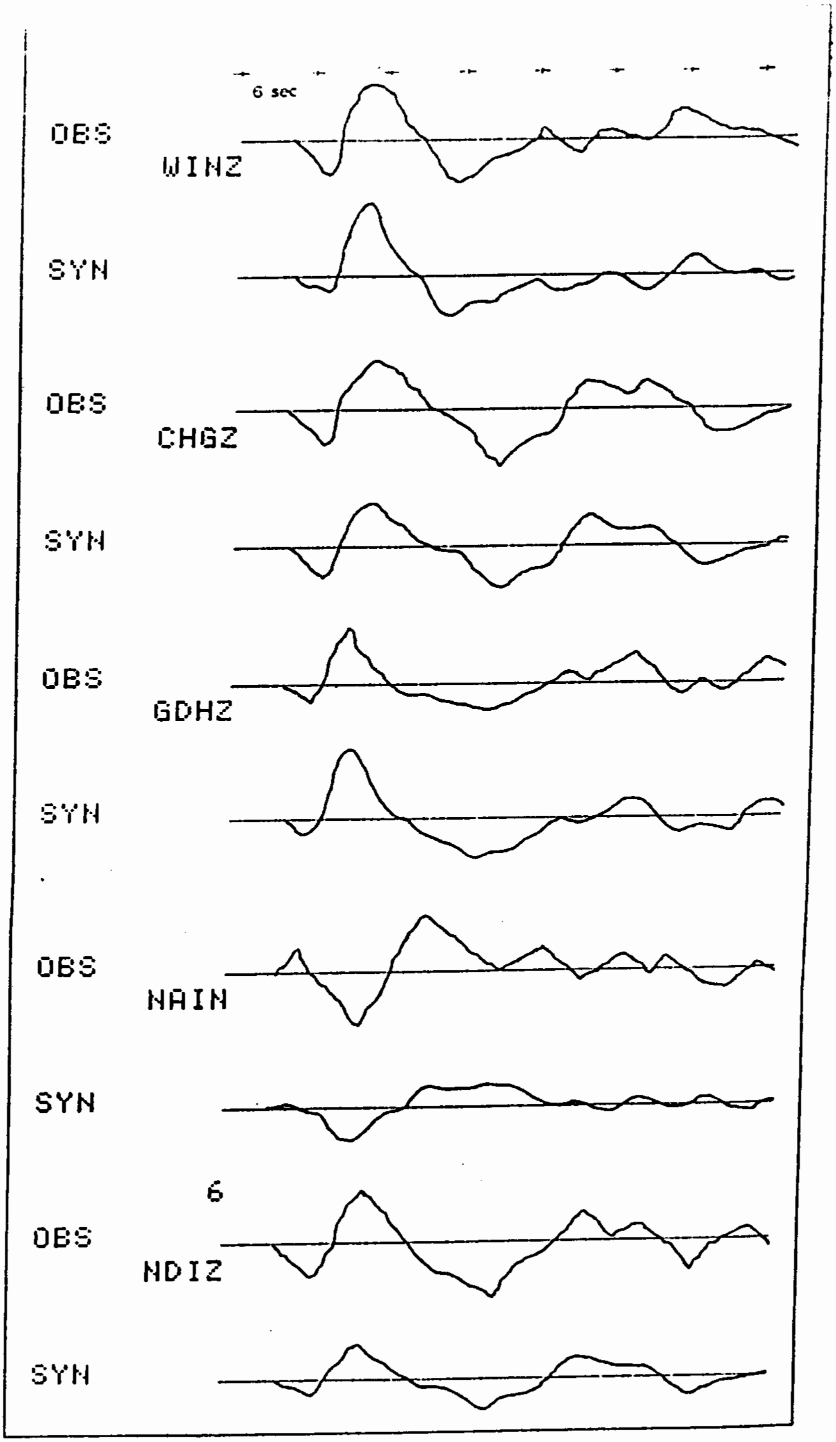

FIGURE 10: The 1981 Corinth earthquake sequence (aftershock of the 4 March). Comparison between observed and synthetic seismograms.

TABLE 3: Aftershock of the 4 March, 1981. Subevent sequence on the fault plane.

No	Onset time(S)	Location X(km)	Location Y(km)	Seismic Moment rate ($x10^{25}$dyne cm)	Seismic Moment ($x10^{25}$dyne.cm)
1	0.0	0.0	0.0	0.3922E-01	0.2745E+00
2	3.6	10.0	-20.0	0.3010E-02	0.2107E-01
3	4.8	-20.0	20.0	0.4048E-02	0.2834E-01
4	4.8	20.0	-20.0	0.6982E-02	0.4887E-01
5	11.2	-20.0	-10.0	0.6862E-02	0.4803E-01
6	12.3	20.0	0.0	0.4563E-02	0.3194E-01
7	13.7	0.0	10.0	0.3149E-02	0.2204E-01
8	17.4	-20.0	20.0	0.6786E-02	0.4750E-01
9	19.3	-10.0	0.0	0.5227E-02	0.3659E-01
10	20.2	10.0	20.0	0.1793E-02	0.1255E-01
11	21.3	20.0	-20.0	0.6221E-02	0.4355E-01
12	22.1	-20.0	20.0	0.1955E-02	0.1368E-01
13	28.8	-20.0	-10.0	0.8899E-02	0.6229E-01
14	29.1	20.0	0.0	0.4465E-02	0.3126E-01
15	31.1	20.0	0.0	0.8476E-02	0.5933E-01
16	31.1	20.0	10.0	0.2361E-02	0.1653E-01
17	33.6	0.0	-20.0	0.2679E-02	0.1875E-01
18	34.4	20.0	0.0	0.5884E-02	0.4119E-01
19	36.1	20.0	0.0	0.3622E-02	0.2535E-01
20	37.2	20.0	0.0	0.7625E-02	0.5337E-01
21	38.9	20.0	0.0	0.5179E-02	0.3626E-01
22	44.0	-20.0	20.0	0.4185E-02	0.2930E-01
23	49.3	0.0	-20.0	0.2343E-02	0.1640E-01
24	54.9	-20.0	-20.0	0.2520E-02	0.1764E-01
25	56.8	20.0	0.0	0.4952E-02	0.3466E-01

TOTAL SEISMIC MOMENT=$1.07x10^{25}$

It has been shown that the source process was very complex and each shock included several individual subevents with different onset times, location on the fault plane, and seismic moments. In the analysis only WWSSN long period seismograms were used in the epicentral distance range 45°to 90°. Thus, the overall complexity of the observed wave-forms is wholly attributed to the source complexity. Only 3 min duration have been digitized.

Calculated rupture patterns show reasonably good consistency with the observed surface breaks.

Large, shallow earthquakes in the Gulf of Corinth region tend to occur in closely related pairs and are typically separated by a few hours or several days in time and by 25-40 km in space. In the last sequence of 1928, the first shock occured on Apr. 22 (19h59m155) (Ms=5.2), the main shock on Apr. 22 (20h13m46s) (Ms=6.3) and the largest aftershock on Apr. 25 (00h31m 18s) (Ms=5.2).

JACKSON et al., 1982 based on fault parameters estimated from both teleseismic and field observations suggest a stress drop of 33.6, 7.0, and 4.5 bars for the main, 25 February and 4 March shocks,respectively. KIM et al., 1984 based on body-wave analysis obtained 10.2, 8.0, and 6.6 bars, respectively. The striking features of the Corinth sequence are the low stress drops of the main shock and its two largest aftershocks as well as the easterly migration of the seismicity. The low stress drops and the long durationof the obtained source time functions suggest an overall slow evergy release during the earthquake sequence.

REFERENCES

CIPAR, J. 1979. Source process of the Haicheng, China earthquake from observations of P and S waves, Bull. Seism. Soc. Am, 69, 1903-1916.

CHUNG, W-Y. and CIPAR, 1983. Source modeling of the Hsingtai, China earthquakes of March 1966, Physics of the Earth and Planetary Interiors, 33, 111-125.

DAS, S. and K.AKI, 1977. Fault plane with barriers: a versatile earthquake model, J.Geophys. Res. 82, 5648-5670.

DZIEWONSKI, A., M., and J., H., WOODHOUSE, 1983. An experiment in systematic study of global seismicity: centroid-moment tensor solutions for 201 moderate and large earthquakes of 1981, J. Geophys. Res. 88, 3247-3271.

FUKAO, Y., and M.FURUMOTO, 1975. Foreshocks and multiple shocks of large earthquakes, Phys. of the Earth and Planetary Interiors, 10, 355-368.

JACKSON, J.A., J.GAGNEPAIN, G.HOUSEMAN, G.C.P.KING, P.PAPADIMITRIOU, C.SOUFLERIS, and J.VIRIEUX, 1982. Seismicity, normal faulting, and the geomorphological development of the Gulf of Corinth (Greece): the Corinth earthquakes of February and March 1981, Earth and Planetary Science Letters, 57, 377-397.

KANAMORI, H. and STEWART, G.S. 1978. Seismological aspects of the Guatemala earthquake of February 21, 1977, J.Geophys.Res. 83, 3427-3434.

KIM, W.-Y., KULHANEK, O. and MEYER, K. 1984. Source processes of the 1981 Gulf of Corinth earthquake sequence from body-wave analysis, Bull.Seis.Soc.Am., 74, 459-477.

KIKUCHI, M. and H.KANAMORI, 1982. Inversion of complex waves, Bull. Seism. Soc. Am. 72, 491-506.

KIKUCHI, M. and K.SUDO, 1984. Inversion of teleseismic P-Waves of the Izu-Oshima, Japan earthquake of January 14, 1985, J.Phys. Earth, 23, 161-171.

LANGSTON, C.A. and D.Y. HELMBERGER, 1975. A procedure for modelling shallow dislocation sources, Geophys. J.R. astr. Soc. 42, 117-130.

LAY, T. and H.KANAMORI, 1980. Earthquake douplets in the Solomon islands, Phys. of the Earth and Planetary Interiors, 21, 283-304.

MIKUMO, T. and T. MIYATAKE, 1978. Dynamic rupture process on a three-dimensional fault with non-uniform frictions, and near field seismic waves, Geophys. J.R.astr. Soc. 54, 417-438.

MORI, J. and K. SHIMAZAKI, 1984. High stress drops of short-period subevents from the 1968 Tokachi-Oki earthquake as observed on strong-motion records, Bull. Seism. Soc. Am. 74, 1529-1544.

PAPAZACHOS, B.C., P.E. COMNINAKIS, E.E. PAPADIMITRIOU, and E.M. SCORDILIS, 1984. Properties of the February-March 1981 seismic sequence in the Alkyonides gulf of Central Greece, Annales Geophysicae, 2, 537-544.

WU, F.T., and H. KANAMORI, 1975. Source mechanism of February 4, 1965, Rat Island earthquake, J.Geophys. Res. 78, 6082-6092.

WYSS, M. and J.N., BRUNE, 1967. The Alaska earthquake of 28 March 1964: A complex multiple rupture, Bull. Seismol. Soc. Am. 57, 1017-1023.